Design of a broadband highly dispersive pure silica photonic crystal fiber

Harish Subbaraman,[1] Tao Ling,[1] YongQiang Jiang,[1] Maggie Y. Chen,[2] Peiyan Cao,[1] and Ray T. Chen[1,*]

[1]Microelectronic Research Center, Department of Electrical and Computer Engineering, The University of Texas at Austin, Austin, Texas 78758, USA

[2]Omega Optics, Incorporated, 10435 Burnet Road, Suite 108, Austin, Texas 78758

*Corresponding author: chen@ece.utexas.edu

Received 14 November 2006; revised 22 January 2007; accepted 26 January 2007; posted 21 February 2007 (Doc. ID 77069); published 15 May 2007

A highly dispersive dual-concentric-core pure silica photonic crystal fiber is designed with a maximum chromatic dispersion value of about −9500 ps/(nm km) around the 1.56 μm wavelength region and a full width at half-maximum (FWHM) of 55 nm. The change in the dispersion–bandwidth product as a function of period is carefully studied by using the plane wave expansion method. The coupled mode theory matches well with the plane wave expansion method that was used to simulate the chromatic dispersion. This kind of a photonic crystal fiber structure is suitable for high-dispersion application in phased array antenna systems based on photonic crystal fiber arrays. © 2007 Optical Society of America

OCIS code: 060.2280.

1. Introduction

In the past decade, there has been an increasing use of lasers operating at $\lambda = 1.55$ μm in optical communication systems. This shift in the operating wavelength from 1.31 to 1.55 μm is due to the presence of a low-loss window in silica fibers and due to the invention of erbium-doped fiber amplifiers operating in the same wavelength window [1]. Erbium-doped fiber amplifiers perform an in-line optical amplification of the signal, thus enabling repeaterless transmission for distances greater than a few hundred kilometers. These amplifiers also exhibit excellent noise figures and are compatible with many of the existing components [2]. However, at 1.55 μm, the fibers exhibit a chromatic dispersion of about 17 ps/nm/km [3]. This value is very small for any practical application in true time delay systems.

Fibers designed for dispersion compensation in optical communication have shown that very high values of dispersion ($D > -100$ ps/nm/km) can be achieved in very short lengths of fiber [4]. The dispersion-compensating fibers should have a high negative dispersion coefficient while maintaining minimum losses and low cost. A true time delay unit based on the above mentioned fiber can be used in phased array antenna systems. Since the first working model was demonstrated in the year 1996, photonic crystal fibers [5] (PCFs), fibers with an array of periodic air holes running down the length of the fiber, have gained increasing popularity due to their unique properties such as endless single-mode operation [6], high nonlinearity [7], and ultralow loss [8,9]. PCF structures can be designed to have higher negative dispersion values compared with conventional dispersion compensating fibers [10–12]. These highly dispersive PCFs have a potential for high-dispersion applications such as dispersion compensation to reduce length, payload, and loss [10,13]. Another important application for highly dispersive PCFs is for true time delay elements in phased array antenna systems. This was demonstrated by Jiang *et al.* [14–16]. By using PCFs as true time delay elements, the fiber's total length can be decreased proportionally, leading to compact device structures suitable for airborne and spaceborne applications. Various groups from

0003-6935/07/163263-06$15.00/0

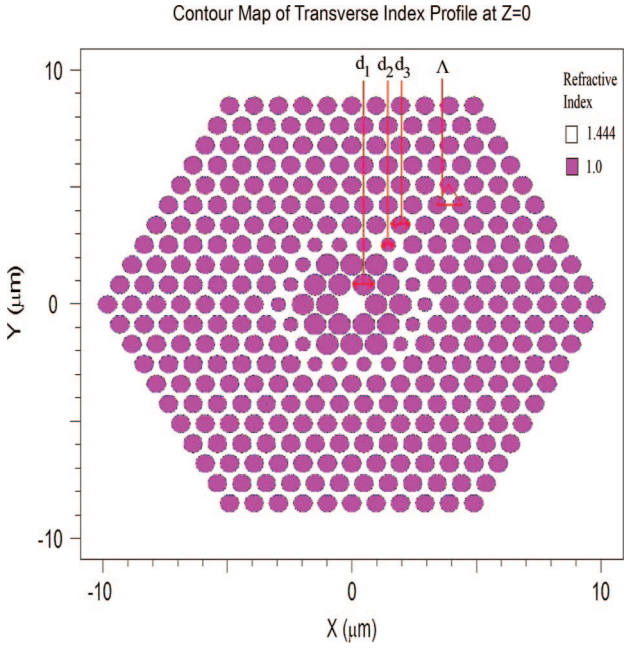

Fig. 1. (Color online) Cross section of the designed dual concentric core PCF.

all over the world have been working on tweaking the peculiar properties of PCFs to achieve high negative dispersion coefficients [10,12] and low-loss structures. Although most of the methods have been able to achieve very high negative dispersion values, the bandwidth is strictly limited, resulting in a relatively small dispersion–bandwidth product. We present the design for a dual-concentric-core PCF [17] to achieve a very high negative dispersion coefficient of about −9500 ps/nm/km, with a full width at half-maximum of 55 nm. A cross section of the designed fiber is shown in Fig. 1; d_1, d_2 denote the diameters of the first and second air-hole rings, which form the inner cladding; d_3 denotes the diameter of the third air-hole ring, which forms the second core. The rest of the air-hole rings (fourth–tenth rings) form the outer cladding region. The period of the air holes is given by Λ. The area at the center, determined by the first air-hole ring diameter and the period, forms the center core. The research presented herein has the highest value dispersion–bandwidth product reported thus far to our knowledge. It also has a high dispersion value that is an improvement by a factor of 5 over previous designs [17] and is a promising candidate for applications requiring compact systems for broadband phased array antennas.

2. Theory and Design of a Dual-Concentric-Core PCF

The mechanism of a dual concentric-core PCF is similar to that of a directional coupler [18]. First, we introduce the coupled mode theory for dual-core PCFs [12]. The central core and the outer core behave as two parallel waveguides, and the high dispersion is from the coupling between the two waveguides. By expanding the propagation constants, β, of the modes in the isolated waveguides around the phase-matched frequency using Taylor's series, we get [18]

$$\beta_i(\omega) \approx \beta(\omega_p) + (\omega - \omega_p)\frac{d\beta_i}{d\omega}\bigg|_{\omega=\omega_p} + \frac{(\omega-\omega_p)^2}{2}\frac{d^2\beta_i}{d\omega^2}\bigg|_{\omega=\omega_p}, \quad (1)$$

where $i = 1, 2$ represents the inner and the outer waveguide, respectively, and ω_p represents the phase-matched frequency. From the coupled mode theory, we know that coupling of the individual modes can generate two supermodes, whose propagation constants can be written as [18]

$$B_\pm = \frac{1}{2}\{[\beta_1(\omega) + \beta_2(\omega)] \pm \sqrt{[\beta_1(\omega) - \beta_2(\omega)]^2 + 4\kappa^2}\}, \quad (2)$$

where κ is the coupling constant between the two waveguides. We can insert Eq. (1) into Eq. (2) and differentiate the result twice with respect to angular frequency. Supposing that the two waveguides'

$$\frac{d^2\beta}{d\omega^2}\bigg|_{\omega=\omega_p}$$

are all very small numbers (this term is determined mainly by the material dispersion of waveguide, and so it must be a very small term), we get the group-velocity dispersion as

$$\frac{d^2\beta_\pm}{d\omega^2} = \pm\frac{1}{4\kappa}\left(\frac{d\beta_1}{d\omega} - \frac{d\beta_2}{d\omega}\right)^2 \times\left[\frac{(\omega-\omega_p)^2}{4\kappa^2}\left(\frac{d\beta_1}{d\omega} - \frac{d\beta_2}{d\omega}\right)^2 + 1\right]^{-3/2}. \quad (3)$$

The dispersion parameter is normally written as [1]

$$D = -\frac{\lambda}{c}\frac{d^2 n_{\text{eff}}}{d\lambda^2} = -\frac{2\pi c}{\lambda^2}\frac{d^2 B}{d\omega^2}. \quad (4)$$

Using Eqs. (3) and (4), we get

$$D = \mp\frac{\pi}{2c\kappa}\left(\frac{dn_1}{d\lambda} - \frac{dn_2}{d\lambda}\right)^2 \times\left[\frac{\pi^2}{\kappa^2}\frac{(\lambda-\lambda_p)^2}{\lambda_p^2}\left(\frac{dn_1}{d\lambda} - \frac{dn_2}{d\lambda}\right)^2 + 1\right]^{-3/2}. \quad (5)$$

From Eq. (5), we see that the dispersion value reaches its maximum value when λ is equal to λ_p and is given by

$$D_{\text{Max}} = \mp\frac{\pi}{2c\kappa}\left(\frac{dn_1}{d\lambda} - \frac{dn_2}{d\lambda}\right)^2. \quad (6)$$

The FWHM can be derived from Eqs. (5) and (6) as

$$\Delta\lambda = 0.766 \times \frac{2\kappa\lambda_p}{\pi}\left|\left(\frac{dn_1}{d\lambda} - \frac{dn_2}{d\lambda}\right)^{-1}\right|. \quad (7)$$

From Eqs. (6) and (7), we see that the dispersion value depends mainly on the coupling constant κ and

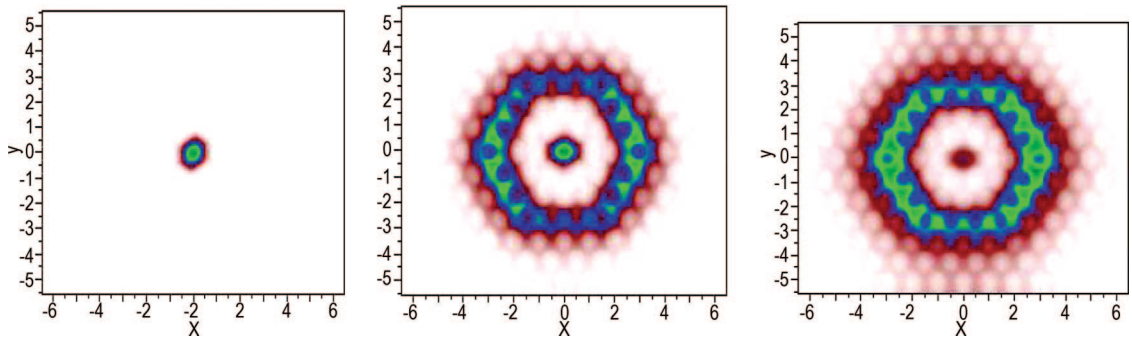

Fig. 2. (Color online) Mode profile at (a) $\lambda < \lambda_p$, (b) $\lambda \approx \lambda_p$, (c) $\lambda > \lambda_p$.

the difference of $dn/d\lambda$ between the inner and the outer core. The bandwidth is dependent on the phase-match wavelength (λ_p), the coupling constant κ, and the difference of $dn/d\lambda$ between the inner and the outer core.

There is a trade-off between the maximum dispersion value and the FWHM. If we multiply Eq. (6) by Eq. (7), we can get a dispersion–bandwidth product that is independent of the coupling constant (κ). This product can be defined as a figure of merit for our structure:

$$|D_{\mathrm{Max}}\Delta\lambda| = 0.766 \times \frac{\lambda_p}{c}\left|\frac{dn_1}{d\lambda} - \frac{dn_2}{d\lambda}\right|. \tag{8}$$

Equation (8) shows that the product depends on the phase-match wavelength, and we further define

$$T = \left|\frac{dn_1}{d\lambda} - \frac{dn_2}{d\lambda}\right|,$$

which is the difference of $dn/d\lambda$ between the inner and the outer core. If our interest is around a specific wavelength, say $\lambda_p = 1.56\ \mu$m, then the product just depends on the value of T. To maximize the dispersion–bandwidth product, we need to increase T as much as possible.

The parameters of the fiber were carefully chosen to make the respective modes have a phase match at a wavelength (λ_P) close to 1.56 μm. The redistribution of modal fields with a variation in wavelength is shown in Fig. 2. When the wavelength is shorter than the phase-match wavelength ($\lambda < \lambda_p$), the field is essentially confined in the inner core [Fig. 2(a)]. Around the phase-match wavelength ($\lambda \approx \lambda_p$), a part of the field is in the inner core and a part is in the outer core [Fig. 2(b)]. When the wavelength is longer than the phase-match wavelength ($\lambda > \lambda_p$), most of the power spreads to the outer core and is effectively guided in the outer core [Fig. 2(c)]. This modal field redistribution makes the effective index change greatly with the wavelength, and thus near the phase-match wavelength the dispersion of the dual concentric core fiber will be very high.

3. Simulation and Results

At the phase-match wavelength around 1.56 μm, the effect of varying the period (Λ) on $dn/d\lambda$ and the dispersion–bandwidth product was carefully studied by using the fully vectorial plane wave expansion (PWE) method [19], wherein, the solutions to Maxwell's equations are found by expanding the fields in terms of plane waves and applying Bloch's theorem, along with the principle of orthogonality of modes. Although the fully vectorial PWE method is extremely accurate for periodic structures without defects, it is only approximately accurate for periodic structures with defects—assuming that a proper supercell containing the defect is selected for calculations. A more detailed explanation can be found in a paper by Ho *et al.* [19]. The simulations are done using RSoft BandSOLVE software [20] that is based on the full vectorial PWE method. For our design, a supercell of size 10×10, instead of a unit cell, is implemented for periodic boundary conditions. In Fig. 3, the curve marked with filled squares shows the $dn/d\lambda$ change of the inner core with respect to the change in the period, and the curve marked with the open squares shows the same variation for the outer core around the wavelength 1.56 μm. We can clearly see from the graph that the inner core $dn/d\lambda$ changes linearly with a change in the period and that a smaller period gives a larger $dn/d\lambda$ value. This is because a smaller period gives a smaller inner core, and thus the confinement in the inner core will become weaker. This makes the effective index in the inner core more sensitive to the wavelength change, which means that the absolute value of $dn/d\lambda$ increases significantly when the period is decreased. For the outer core, the $dn/d\lambda$ value changes very little with the period. This

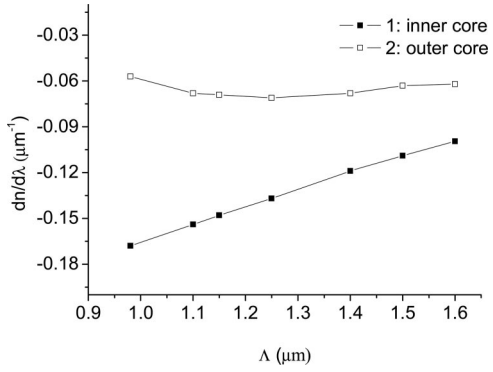

Fig. 3. Variation of $dn/d\lambda$ with respect to the period (Λ).

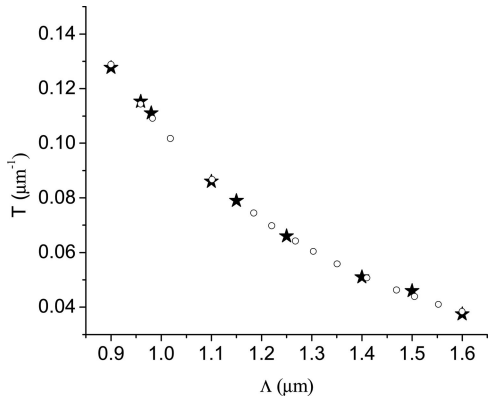

Fig. 4. Relationship between T and period (Λ).

is because the outer core has a ringlike structure, and this kind of structure's confinement ability is stronger compared with the inner core's rod structure. So we can see that the $dn/d\lambda$ of the outer core guided mode is almost unchanged, and the value is around $-0.065\ \mu m^{-1}$; but when the period is smaller than 1 μm, the confinement in the outer core also becomes weaker, and the $dn/d\lambda$ value becomes smaller. The value of T can be calculated from Fig. 3, and the result is shown in Fig. 4. We find that the value of T decreases with an increase in the period, and this is contributed mainly by the inner core's $dn/d\lambda$ change. The curve marked with stars is the calculation result, and the curve marked with circles is a fit to the calculation result. We find that the value of T exponentially decays with an increase in the period of the holes, and the decay constant is about 0.431 μm. This also means that the dispersion–bandwidth product decays exponentially as the period is increased. Thus this product increases as the period is decreased.

From the above discussion we find that the period (Λ) plays a vital role in achieving broadband operation along with a very high dispersion value. By designing structures with very small periods, we can achieve very high dispersion–bandwidth products. However, it becomes difficult to control the diameter of the air holes over such small dimensions. By choosing a period of 0.98 μm, we are almost hitting the limits of manufacturability. To satisfy the high dispersion–bandwidth requirement and manufacturing feasibility simultaneously, a dual-concentric-core pure silica PCF with period = 0.98 μm is designed to have a maximum dispersion value of about −9500 ps/nm/km and bandwidth of about 55 nm.

The inner core is made of pure silica, surrounded by an inner cladding made of two air-hole rings with of diameter d_1, followed by an outer core with diameter d_2, and then by an outer cladding with diameter d_3. Since we are hitting the limit of manufacturability at a period of 0.98 μm, we chose this value for the period and simulated structures with various parameter values. A structure with values of $d_1/\Lambda = 0.90$, $d_2/\Lambda = 0.76$, and $d_3/\Lambda = 0.59$ gave us a dip in the dispersion curve around 1.56 μm. These values were obtained after many trial values were simulated. Each parameter is independent of the others. To see the effect of these parameters on the dispersion curve, each parameter was varied independently, while the remaining parameters were kept at the above mentioned values. The results are shown in Figs. 5(b), 5(c), and 5(d). It can be seen from these figures that any small deviation in the parameter can totally change the dispersion curve in terms of magnitude and position. Therefore the parameters need to be strictly controlled while drawing the fibers. This sets a limit on the manufacturability. The dependence of dispersion on Λ is shown in Fig. 5(a). As discussed previously, it can be seen that the value of dispersion decreases as the period is increased. The dip also changes its position on the wavelength scale. In our design, we have used two air-hole rings between the inner and the outer core instead of one as given by Gérôme *et al*. [17]. As the number of air-hole rings increases between the two cores, the value of dispersion becomes larger, but the bandwidth becomes narrower as shown in Fig. 6. We choose two air-hole rings, as it gives a high value of dispersion along with a reasonable bandwidth of operation suitable for our application. The variation in the effective index of the fundamental mode with wavelength is studied by using the PWE method [19]. In Fig. 7, the curves marked with − and + show the effective refractive index change with the wavelength in the inner and the outer core, respectively. The curve marked with stars is due to the combined effect of the concentric cores; it connects the inner core's $dn/d\lambda$ and outer core's $dn/d\lambda$ and is dependent mainly on the coupling constant between the inner and the outer core. This curve predominantly controls the shape of the resulting dispersion curve. We can also see that the two individual core curves are like the asymptotes to the combined curve. This means that, for a wavelength greater than the phase-match wavelength, the mode is just like being confined in the outer core and cannot feel any effect from the inner core and vice versa. To use Eq. (4) to calculate the net chromatic dispersion of the structure, we perform a second differential on the curve marked with stars with respect to the wavelength and multiply by $-\lambda/c$. The result of our calculation is shown in Fig. 8 as a curve marked with solid squares. From the figure, we see that the maximum value of dispersion achieved is around −9500 ps/nm/km, and the FWHM is about 55 nm near a wavelength of 1.56 μm.

There are still some problems with this kind of design. Because the small period makes the inner core's diameter very small, ~1.5 μm, the coupling from a standard single-mode fiber to this fiber becomes difficult. There are fiber companies that can handle this problem. They use an intermedia fiber coupler from single-mode fiber to a taper fiber, followed by coupling from tapered fiber to the small-core PCF. This way, the total coupling loss can be brought down to less than 3 dB.

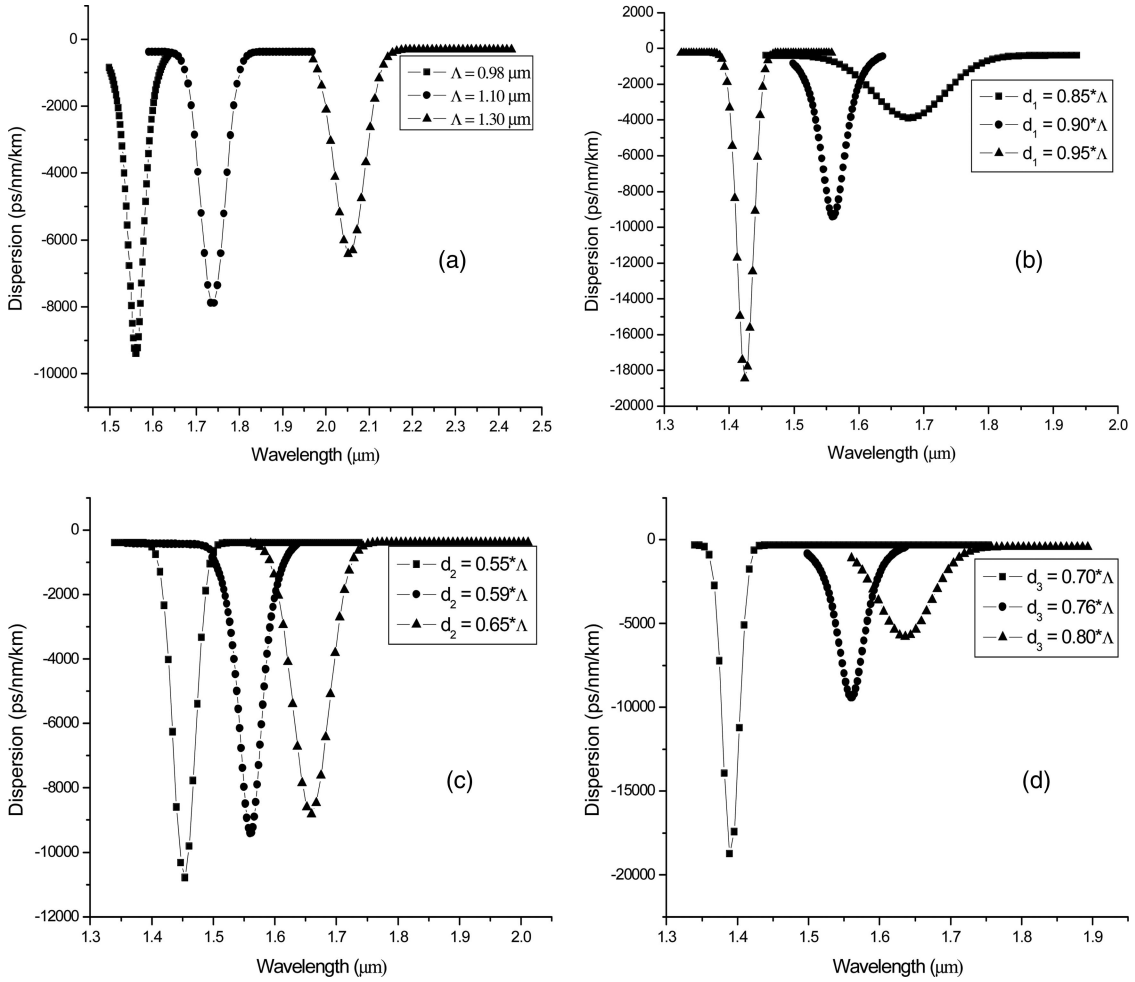

Fig. 5. Variation of the dispersion value and the shift observed due to (a) variation in the pitch, (b) variation of d_1, (c) variation of d_2, and (d) variation of d_3, while keeping the other parameters as in the given design in each case.

The finite-difference beam propagation method [20–22] (BPM) was used to calculate the two mode patterns in the inner and the outer core, and the overlap integral method was used to calculate the coupling constant between the two cores. The simulations were done using the RSoft BeamPROP software package [20]. The software can compute the mode patterns, given a refractive index profile and an input field. Apart from calculating the mode patterns, this method can also be used to calculate the

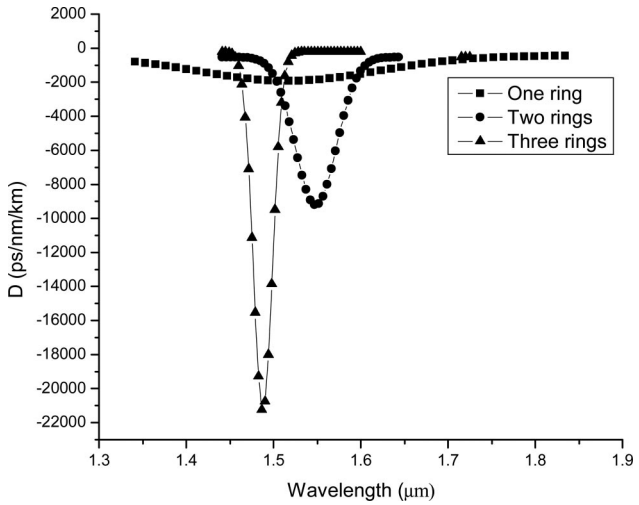

Fig. 6. Variation of dispersion with number of air-hole rings between the inner and the outer core.

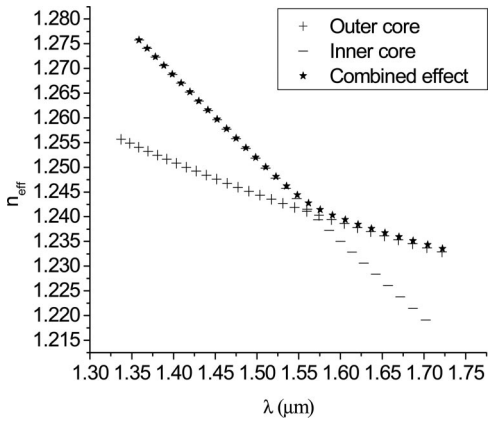

Fig. 7. Effect of coupling on the effective refractive index.

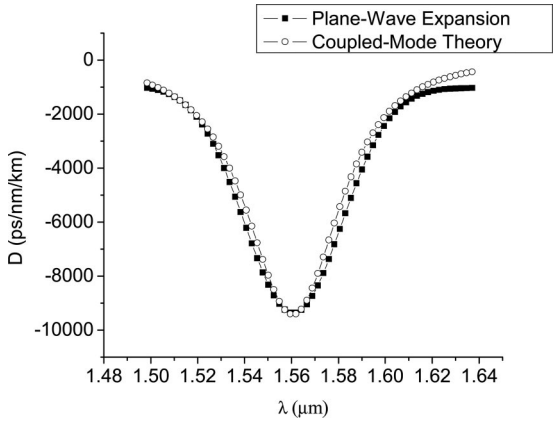

Fig. 8. Relationship between the dispersion value D and wavelength, and comparison of PWE and coupled mode theory results.

radiation or leaky modes modes [20]. The coupling factor was found to be $\kappa = 2\pi \times 0.00167/\lambda_p = 0.00673\ \mu m^{-1}$. Coupled mode theory was employed to obtain the curve between the dispersion and the wavelength. The PWE [19] is compared with that of the coupled mode theory [3] in Fig. 8, and the results are found to be in good agreement with each other. This kind of broadband, highly negative dispersion fiber can be used in radar applications.

4. Conclusion

We have described the coupled mode theory in a dual-concentric-core photonic crystal fiber (PCF) and shown that the dispersion property (T value) depends mainly on the difference of $dn/d\lambda$ between the inner and the outer cores. The change in dispersion property with period was carefully studied by the plane wave expansion (PWE) method. We found that smaller periods gave a larger value of T, and this was due mainly to the inner core's large $dn/d\lambda$ value. By choosing a period of 0.98 μm, we got a dual-concentric-core pure silica PCF design with a maximum chromatic dispersion value of about −9500 ps/nm/km and FWHM around 55 nm in the 1.56 μm wavelength window. We also found that the coupled mode theory matched well with the PWE method that we used in calculating the chromatic dispersion curve. This kind of broadband, highly dispersive PCF is suitable for applications requiring compact phased array antennas.

References

1. J. L. Auguste, J. M. Blondy, J. Maury, J. Marcou, B. Dussardier, G. Monnom, R. Jindal, K. Thyagarajan, and B. P. Pal, "Conception, realization, and characterization of a very high negative chromatic dispersion fiber," Opt. Fiber Technol. **8,** 89–105 (2002).
2. E. Desurvire, *Erbium-Doped Fiber Amplifiers* (Wiley, 1994).
3. F. Gérôme, J. L. Auguste, J. Maury, J. M. Blondy, and J. Marcou, "Theoretical and experimental analysis of a chromatic dispersion compensating module using a dual concentric core fiber," J. Lightwave Technol. **24,** 442–448 (2006).
4. B. Jopson and A. Gnauck, "Dispersion compensation for optical fiber systems," IEEE Commun. Mag. **33,** 96–102 (1995).
5. J. C. Knight, T. A. Birks, P. St. J. Russell, and D. M. Atkin, "All-silica single-mode optical fiber with photonic crystal cladding," Opt. Lett. **21,** 1547–1549 (1996).
6. T. A. Birks, J. C. Knight, and P. St. J. Russell, "Endlessly single-mode photonic crystal fiber," Opt. Lett. **22,** 961–963 (1997).
7. Z. Yusoff, J. H. Lee, W. Belardi, T. M. Monro, P. C. Teh, and D. J. Richardson, "Raman effects in a highly nonlinear holey fiber: amplification and modulation," Opt. Lett. **27,** 424–426 (2002).
8. K. Tajima, J. Zhou, K. Nakajima, and K. Sato, "Ultralow loss and long length photonic crystal fiber," J. Lightwave Technol. **22,** 7–10 (2004).
9. M. Koshib and K. Saitoh, "Simple evaluation of confinement losses in holey fibers," Opt. Commun. **253,** 95–98 (2005).
10. S. K. Varshney, K. Saitoh, and M. Koshiba, "A novel design for dispersion compensating photonic crystal fiber Raman amplifier," IEEE Photon. Technol. Lett. **17,** 2062–2064 (2005).
11. Y. Jiang, T. Ling, L. Gu, W. Jiang, X. Chen, and R. T. Chen, "Highly dispersive photonic crystal waveguides and their applications in optical modulators and true-time delay lines," Proc. SPIE **6128,** 61280Y (2006).
12. S. K. Varshney, T. Fujisawa, K. Saitoh, and M. Koshiba, "Design and analysis of a broadband dispersion compensating photonic crystal fiber Raman amplifier operating in S-band," Opt. Express. **14,** 3528–3540 (2006).
13. B. J. Mangan, F. Couny, L. Farr, A. Langford, P. J. Roberts, D. P. Williams, M. Banham, M. W. Mason, D. F. Murphy, E. A. M. Brown, and H. Sabert, "Slope-matched dispersion-compensating photonic crystal fibre," in *Conference on Lasers and Electro-Optics, 2004 (CLEO)* (Optical Society of America, 2004), pp. 1069–1070.
14. Y. Jiang, Z. Shi, B. Howley, X. Chen, M. Y. Chen, and R. T. Chen, "Delay-time-enhanced photonic crystal fiber array for wireless communications using two-dimensional X-band phased-array antennas," Opt. Eng. **44,** 125001 (2005).
15. Y. Jiang, B. Howley, Z. Shi, Q. Zhou, R. T. Chen, M. Y. Chen, G. Brost, and C. Lee, "Dispersion-enhanced photonic crystal fiber array for a true time-delay structured X-band phased array antenna," IEEE Photon. Technol. Lett. **17,** 187–189 (2005).
16. Y. Jiang, Z. Shi, B. Howley, and R. T. Chen, "Highly dispersive photonic crystal fibers for true-time-delay modules of an X-band phased array antenna," Proc. SPIE **5360,** 253–258 (2004).
17. F. Gérôme, J. L. Auguste, and J. M. Blondy, "Design of dispersion-compensating fibers based on a dual-concentric-core photonic crystal fiber," Opt. Lett. **29,** 2725–2727 (2004).
18. U. Peschel, T. Peschel, and F. Lederer, "A compact device for highly efficient dispersion compensation in fiber transmission," Appl. Phys. Lett. **67,** 2111–2113 (1995).
19. K. M. Ho, C. T. Chan, and C. M. Soukoulis, "Existence of a photonic gap in periodic dielectric structures," Phy. Rev. Lett. **65,** 3152–3155 (1990).
20. RSoft Photonics CAD Suite, Version 5.1.7.
21. R. Scarmozzino, A. Gopinath, R. Pregla, and S. Helfert, "Numerical techniques for modeling guided-wave photonic devices," J. Sel. Top. Quantum Electron. **6,** 150–162 (2000).
22. R. Scarmozzino and R. M. Osgood, Jr., "Comparison of finite-difference and Fourier-transform solutions of the parabolic wave equation with emphasis on integrated-optics applications," J. Opt. Soc. Am. A **8,** 724–731 (1991).